

# Hydraulic jumps on an incline

JEAN-LUC THIFFEAULT<sup>1,2</sup>  
AND ANDREW BELMONTE<sup>3</sup>

<sup>1</sup> Department of Mathematics, University of Wisconsin, Madison, WI 53706, USA

<sup>2</sup> Institute for Mathematics and its Applications, University of Minnesota, Minneapolis, MN 55455, USA

<sup>3</sup> The W. G. Pritchard Laboratories, Department of Mathematics, Penn State University, University Park, PA 16802, USA

When a fluid jet strikes an inclined solid surface at normal incidence, gravity creates a flow pattern with a thick outer rim resembling a parabola and reminiscent of a hydraulic jump. There appears to be little theory or experiments describing simple aspects of this phenomenon, such as the maximum rise height of the fluid above the impact point, and its dependence on jet velocity and inclination angle. We address this with experiments, and present a simple theory based on horizontal hydraulic jumps which accounts for the rise height and its scaling, though without describing the shape of the parabolic envelope.

**Key Words:** Hydraulic jumps

---

## 1. Introduction

The description of the hydraulic jump arising from a jet striking a solid surface has been a rich source of fluid dynamical problems for decades. The first fairly complete description is usually attributed to Watson (1964), and his theory has been refined and improved by many authors (for example Bohr *et al.* (1993); Godwin (1993); Bohr *et al.* (1997); Brechet & Néda (1999); Chang *et al.* (2001); Bush & Aristoff (2003)). Experimentally, there are several variants of the problem, such as where the jet strikes a horizontal plate at an oblique angle (Sparrow & Lovell 1980; Rubel 1981; Kate *et al.* 2007), or where the plate is moving (Gradeck *et al.* 2006; Kate *et al.* 2009).

Another important case involves the impact of a jet on a plane inclined with respect to the horizontal, so that there is now a gravitational force tangential to the plane. A profile resembling a parabola is then observed, with a maximum ‘rise distance’ along the plane (figure 1). This rise distance can be associated with the hydraulic jump in the purely horizontal case, although there are differences. A full description of this problem is challenging, partly because of the breaking of axial symmetry, but also due to the necessarily complex flow in the thick ‘rim’ bounding the inner, shallow region. For that reason, most existing models are based on inviscid fluid dynamics (or the opposite extreme of Stokes flow, as in Lister (1992)). Rienstra (1996) first described this situation in terms of the ballistic motion of fluid particles, leading to parabolic trajectories with a parabolic envelope or rim. Such a ballistic model predicts a rise distance of order  $U^2/(2g \sin \theta)$ , where  $U$  is the jet velocity and  $g \sin \theta$  the component of gravity along the plane. In this model the particle trajectories are characteristics of a geodesic equation modified by gravity (Thiffeault & Kamhawi 2008), and these characteristics cross. Edwards *et al.* (2008) used a ‘delta-shock’ model to resolve the crossing of characteristics, which lowers the rise distance to 5/9 of the ballistic value whilst maintaining a near-parabolic outer envelope.

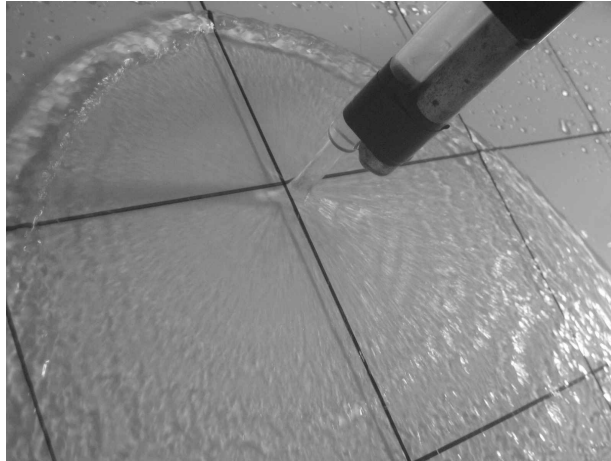


FIGURE 1. Impact of a jet on plane inclined at  $45^\circ$ . The flow rate is  $Q \simeq 119 \text{ cm}^3 \text{ s}^{-1}$  and the rise distance is  $\simeq 7 \text{ cm}$ .

However, in their inviscid model the rise distance still scales in the same way as for the ballistic theory. In their paper Edwards *et al.* (2008) performed one experiment (at  $90^\circ$  inclination angle) and found a significantly lower value of the rise distance than their theory predicted; they expressed hope that faster flow rates might capture the inviscid regime, but this has still to be verified.

In the present paper we account for the discrepancy using a viscous theory, motivated by observations made in a simple experiment. The theory is a straightforward modification of Bohr *et al.* (1993), where the authors matched inner and outer solutions to viscous shallow-water equations to predict the radius of a circular hydraulic jump. To simplify the treatment, we include a component of the gravitational force pointing towards the jet while maintaining the assumption of axial symmetry. The resulting equation correctly captures the dependence of the rise distance on both the jet velocity and inclination angle. The model, however, is not sufficient to address other features of the hydraulic jump, such as the shape of the envelope, or whether the jump closes or has an open (i.e., parabolic-like) shape (see Lebon *et al.* (2008)). The model does not agree as well with experiments at slower rates of flow, as in Bohr *et al.* (1993), or at angles of inclination larger than about  $60^\circ$ .

## 2. Experimental setup and results

We performed a simple experimental study on an inclined hydraulic jump to measure the dependence of the rise distance on flow rate and inclination angle. A large plexiglas sheet is held clamped over a sink at a constant angle, so that the water runs directly off at the edge. This sheet is painted white on one side and marked with a regular 10 cm grid for length calibration. A small pump is used to supply fresh water at a constant flow rate  $Q$ , connected to a straight glass tube by flexible plastic tubing. The glass tube defines the nozzle of the jet, which has an inner diameter  $d = 0.56 \text{ cm}$ . It is fastened to a metal rod that can be adjusted so that the jet strikes the sheet at normal incidence for each value of  $Q$  and inclination angle, while the nozzle itself is kept at a 3.5 cm distance from the sheet. The flow rate was measured after each run by the time taken to fill a one liter beaker for each  $Q$ . Based on this and the nozzle geometry we have an exit velocity  $U \simeq 1\text{--}4 \text{ m/s}$ , with Reynolds number  $Re \simeq 6 \times 10^3\text{--}3 \times 10^4$ .

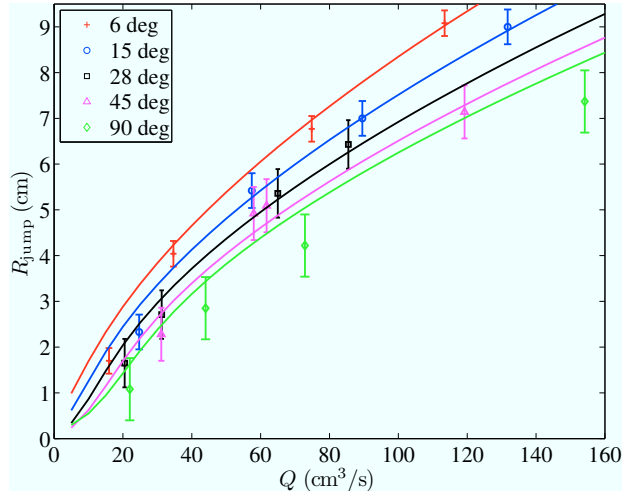


FIGURE 2. Maximum rise distance  $R_{\text{jump}}$ , measured upslope from the center of the jet to the lower edge of the bounding rim. The solid lines come from the theoretical prediction (3.14). The theory works well for moderate angles (not near  $90^\circ$ ) and faster jet speeds.

We inclined the plexiglas at five different angles  $\theta$ , measured with respect to the horizontal:  $\theta = 6^\circ, 15^\circ, 28^\circ, 45^\circ$ , and  $90^\circ$ . At each angle, we varied the flow rate  $Q \simeq 20$ – $150 \text{ cm}^3 \text{ s}^{-1}$ . Finally, from photographs we measured the rise distance  $R_{\text{jump}}$ , which we define as the distance from the center of the jet to the position of the zenith of the hydraulic jump (i.e., the lower part of the rim or envelope at its point of highest rise). Note that at higher  $Q$  and  $\theta$  the flow becomes more unsteady, and the rise distance has larger error bars (in those cases we average the rise distance over time). Figure 2 summarizes the results for the measured  $R_{\text{jump}}$ , which increases with velocity and decreases with  $\theta$ , as one would expect. We now present a simple theory to explain this dependence.

### 3. A simple model

To capture the maximum rise distance of the fluid along the sloping surface, we will model the flow as axisymmetric with a radial force, where the radial force arises from gravity along the slope angle. The radial model is suggested by the radial surface waves visible in figure 1, which appear roughly circular despite the inclination. This simplified model will prove sufficient to capture the scaling of  $R_{\text{jump}}$  with jet velocity and inclination angle. To satisfy mass conservation, one can imagine truncating the surface just past the hydraulic jump, so that fluid can spill out. This model resembles a truncated inverted cone, with the jet hitting the apex, though without the geometrical factors associated with a cone.

Following Bohr *et al.* (1993), we start with the steady, incompressible Navier–Stokes and mass conservation equations in axisymmetric cylindrical coordinates, in the boundary layer approximation:

$$u \frac{\partial u}{\partial r} + w \frac{\partial u}{\partial z} = -g \cos \theta \frac{dh}{dr} - g \sin \theta + \nu \frac{d^2 u}{dz^2}, \quad (3.1a)$$

$$\frac{\partial u}{\partial r} + \frac{u}{r} + \frac{\partial w}{\partial z} = 0, \quad (3.1b)$$

where  $u(r, z)$  and  $w(r, z)$  are respectively the velocity components tangent and perpendicular to the solid surface,  $g$  is gravitational acceleration,  $h$  is the fluid thickness, and

$\nu$  is the kinematic viscosity. The coordinate  $r$  is tangent to the solid surface, and  $z$  is perpendicular to it. The boundary conditions at the bottom and top of the fluid are

$$u = 0, \quad w = 0, \quad \text{at } z = 0; \quad (3.2a)$$

$$\frac{\partial u}{\partial z} = 0, \quad w = u \frac{dh}{dr}, \quad \text{at } z = h(r). \quad (3.2b)$$

Integrating equation (3.1b) gives the mass conservation equation

$$r \int_0^h u(r, z) dz = q \quad (3.3)$$

where  $q = Q/2\pi$ , with  $Q$  the flow rate of the jet. In addition, we must specify the velocity  $u(r_0, z) = u_0(z)$  and height  $h(r_0) = h_0$  at a radius  $r_0$  larger than the jet radius, since the boundary layer equations are not valid directly under the jet. When  $\theta = 0$ , equations (3.1) reduce to those of Bohr *et al.* (1993).

We use the standard hydraulic jump scalings to define dimensionless ‘tilde’ variables:

$$u = \alpha \tilde{u}, \quad \alpha = (c_1^{-1/2} c_2^{1/8}) q^{1/8} \nu^{1/8} (g \cos \theta)^{3/8}, \quad (3.4a)$$

$$w = \beta \tilde{w}, \quad \beta = q^{-1/4} \nu^{3/4} (g \cos \theta)^{1/4}, \quad (3.4b)$$

$$r = \Gamma \tilde{r}, \quad \Gamma = (c_1^{1/2} c_2^{-3/8}) q^{5/8} \nu^{-3/8} (g \cos \theta)^{-1/8}, \quad (3.4c)$$

$$z = \delta \tilde{z}, \quad \delta = (c_2^{1/4}) q^{1/4} \nu^{1/4} (g \cos \theta)^{-1/4}, \quad (3.4d)$$

except that we included the  $\cos \theta$  dependence in the scalings. (We will discuss the dimensionless constants  $c_1$  and  $c_2$  below.) We immediately drop the tildes.

In dimensionless variables, the mass conservation equation (3.3) becomes

$$r \int_0^h u(r, z) dz = 1. \quad (3.5)$$

Upon averaging in the  $z$  direction, equation (3.1a) becomes after integration by parts

$$2u \frac{\partial u}{\partial r} + \frac{1}{r} \overline{u^2} + \frac{h'}{h} u^2 \Big|_{z=h} = -c_1 \left( G + \frac{dh}{dr} \right) - \frac{c_1}{c_2} \frac{1}{h} \frac{\partial u}{\partial z} \Big|_{z=0} \quad (3.6)$$

where the  $z$ -average of a function  $F(r, z)$  is  $\overline{F}(r) = (1/h) \int_0^h F(r, z) dz$ , and we defined

$$G = (c_1^{1/2} c_2^{-5/8}) q^{3/8} \nu^{-5/8} (g \cos \theta)^{1/8} \tan \theta. \quad (3.7)$$

We now assume the separable form

$$u(r, z) = v(r) f'(z/h(r)), \quad (3.8)$$

where  $v = \overline{u}$  is the averaged profile,  $f$  is a given function that describes the vertical structure of the thin layer, with  $f(0) = f'(0) = f''(1) = 0$ ,  $f(1) = 1$ . With this form for  $u$ , the mass conservation integral (3.5) becomes simply  $vh r = 1$ , which gives a relationship between  $v$  and  $h$ . This allows us to derive the two relations

$$2u \frac{\partial u}{\partial r} + \frac{1}{r} \overline{u^2} + \frac{h'}{h} u^2 \Big|_{z=h} = c_1 v \frac{\partial v}{\partial r}, \quad \frac{\partial u}{\partial z} \Big|_{z=0} = c_2 \frac{v}{h}, \quad (3.9)$$

with

$$c_1 = \int_0^1 f'^2(\eta) d\eta \quad \text{and} \quad c_2 = f''(0). \quad (3.10)$$

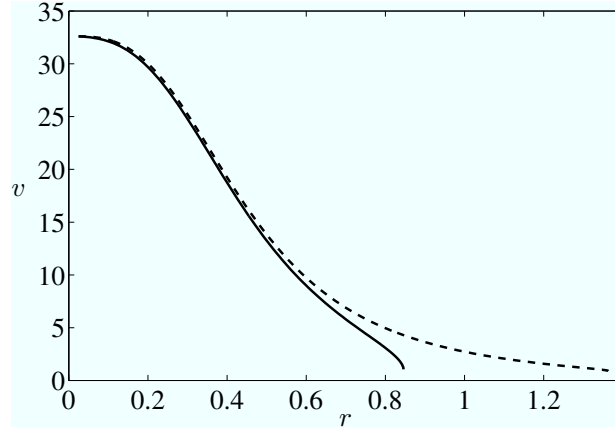


FIGURE 3. Solution of equation (3.12), with boundary condition  $v(.025) = 32.6$  and parameter  $G = 67$  (—), corresponding to the values for figure 1 in dimensionless form. For comparison, the dashed line (- - -) has  $G = 0$ . Both solutions become singular ( $v' \rightarrow -\infty$ ) at  $r_{\text{sing}} = .85$  and 1.36, respectively.

The two relations (3.9) can be used in (3.6) and in the mass conservation integral (3.5) to obtain

$$vv' + h' = -\frac{v}{h^2} - G, \quad vhr = 1. \quad (3.11)$$

For  $G = 0$  the equations (3.11) reduce to those of Bohr *et al.* (1993), which are essentially as derived by Kurihara (1946) and Tani (1949). We combine (3.11) into one ODE for  $v(r)$ :

$$r(1 - rv^3)v' = -(1 - Gr^2v - r^4v^4)v, \quad (3.12)$$

which must be solved together with the flux boundary condition  $v(r_0) = v_0$  at the jet radius  $r_0$ . Note that there is a singularity at  $r = 0$ , and another at  $rv^3 = 1$ . The former is not relevant, since we have  $r > 0$ . The latter will determine the location of the hydraulic jump, which we will associate here with the rise distance. Since  $G = G(Q, \theta)$ , this ODE will have to be solved at each inclination angle and flow rate.

When doing numerical calculations, we will use the parabolic profile

$$f(\eta) = \frac{3}{2}\eta^2 - \eta^3, \quad (3.13)$$

from which equation (3.10) gives  $c_1 = 6/5$ ,  $c_2 = 3$ . A more general approach, for instance using a variable cubic profile as in Bohr *et al.* (1997), doesn't significantly change the scaling.

Let us examine solutions of (3.12) for typical experimental parameters. For the case shown in figure 1,  $Q \simeq 119 \text{ cm}^3 \text{ s}^{-1}$  and  $\theta = 45^\circ$ . The viscosity of water is  $\nu \simeq .01 \text{ cm}^2 \text{ s}^{-1}$  and  $g \simeq 980 \text{ cm s}^{-2}$ . The jet radius is 0.28 cm, and from the flow rate this gives a velocity  $484 \text{ cm s}^{-1}$ . Inserting all this into (3.4), we find a horizontal length scale  $\Gamma = 11.3 \text{ cm}$ , velocity scale  $\alpha = 9.9 \text{ cm s}^{-1}$ , and  $G = 67$ . In dimensionless form, we must now integrate (3.12) from  $r_0 = (.28/11.3) = .025$  with  $v_0 = (2/3)(484/9.9) = 32.6$ . (The  $2/3 = 1/f'(1)$  arises from the choice of a parabolic vertical profile for  $f$ .)

Figure 3 shows the numerical solution (solid line), which becomes singular at  $r = r_{\text{sing}} \simeq .85$ . In dimensional form, the singularity is  $R_{\text{sing}} \simeq 9.6 \text{ cm}$  from the center of the jet. The experimentally-measured value for the lower edge of the hydraulic jump is  $R_{\text{jump}} \simeq 7.2 \text{ cm}$ , with is  $3/4$  of the singularity position. Note that these values are fairly insensitive to the exact jet radius  $r_0$ . For comparison, the numerical solution for  $G = 0$  is also indicated as a dashed line in the figure, with a singularity at a larger value of  $r$ .

The singularity thus appears to occur somewhat beyond the actual position of the jump. To find the position of the jump, we would have to match to the ‘outer’ solution (small  $v$ ) of (3.12), and impose continuity of mass and momentum across the jump, as done in Bohr *et al.* (1993). In addition, Bohr *et al.* (1993) were left with an extra parameter — the location of a singularity of the outer solution — which they fixed by assuming the jet was striking a plate of finite extent, and then moving the singularity to the edge of the plate. We cannot use this approach here: our hydraulic jump actually terminates, which by mass conservation means there must be either backflow or non-axisymmetric flow (or both). Both these effects require more powerful theories or the solution of more complex equations.

On the other hand, since we are only after the scaling of the jump position, the theory we have is enough to uncover this scaling. Bohr *et al.* (1993) observed that their jump location typically occurred at unit radius (in dimensionless variables), somewhat independently of what was happening downstream in the outer solution. This suggests the following approach: fix the ratio of the jump distance to the singularity distance from the center of the jet. In our example above, that ratio was  $3/4$ , but we find  $.76$  fits the set of data slightly better. Hence, we have in dimensional form  $R_{\text{jump}} \simeq .76 r_{\text{sing}} \Gamma$ , or after using in  $\Gamma$  parabolic profile values for the numerical constant,  $c_1^{1/2} c_2^{-3/8} \simeq .73$ :

$$R_{\text{jump}} \simeq .55 r_{\text{sing}}(G, r_0, v_0) \times q^{5/8} \nu^{-3/8} (g \cos \theta)^{-1/8}. \quad (3.14)$$

Here  $r_{\text{sing}}(G, r_0, v_0)$  is obtained by solving the dimensionless ODE (3.12) with initial condition at the jet radius  $v(r_0) = v_0$ , and  $v_0$  is obtained from the dimensionless flow rate by  $v_0 = (2/3)(Q/\pi r_0^2)$ , where the  $2/3$  is for a parabolic vertical profile.

In figure 2 we compare formula (3.14) with experiments at various inclination angles, with the jet always striking the plane normally. We emphasize that the numerical prefactor in (3.14) is fixed, so we are not fitting each data set individually. The theory agrees well with experiments in both velocity and angle, except at low flow rates and at  $90^\circ$  angle. The low flow rate disagreement is not troubling, since it falls outside the theory as pointed out by Bohr *et al.* (1993). The  $90^\circ$  theoretical curve stands out, since it is very close to the theoretical curve for  $45^\circ$ . However, the trend of the  $90^\circ$  curve with  $Q$  is still captured.

Figure 4 shows the singularity position as a function of angle, for a fixed flow rate  $119 \text{ cm s}^{-1}$ . The curve actually has a minimum around  $80^\circ$ , which is unphysical: physically we expect the rise distance to decrease monotonically with angle, though at these large angles of inclination the flow is too unsteady for accurate measurement of the rise distance. We conclude that the theory breaks down for steeper angles: probably backflow becomes important, and the assumption that the the outer solution only weakly affects the jump position breaks down. According to figure 4, the rise distance ceases to increase significantly after about  $60^\circ$ ; however figure 2 shows a significantly higher rise distance for  $90^\circ$  inclination. This suggests that the present theory works well for angles  $\theta \lesssim 60^\circ$ .

#### 4. Conclusions

We have presented simple experiments of the impact of a jet on an inclined plane, and noted the dependence of the maximum rise distance on both flow rate and angle. Though a complete description of this problem is daunting, our simple radial model captures the dependence remarkably well, though less so at smaller flow rates and larger angles. A complete theory would, of course, describe the thickness of the bounding rim, but also predict the critical angle at which the hydraulic jump changes from closed to open (Lebon

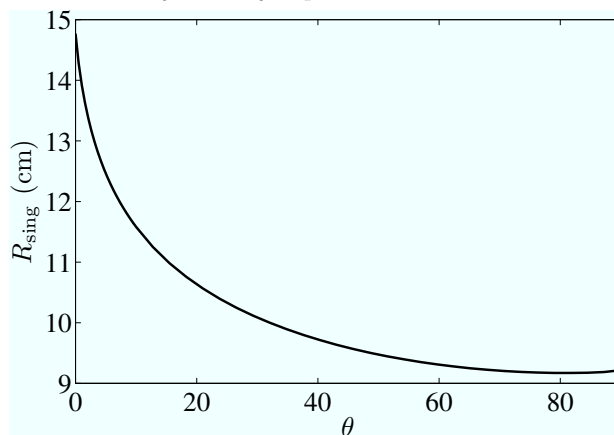


FIGURE 4. Position of the singularity in equation (3.12) as a function of inclination angle, for a fixed flow rate  $Q = 119 \text{ cm s}^{-1}$ . The curve has a minimum around  $80^\circ$ .

*et al.* 2008). Our simple model verifies the need to include viscosity to capture the rise height at these modest flow rates, as pointed out in Edwards *et al.* (2008).

We thank Claudia Cenedese for graciously allowing us to use her lab, as well as Shreyas Mandre, Cecilia Ortiz-Duenas and J. B. Keller for helpful discussions. J-LT and AB are grateful for the hospitality of the 2008 Summer Program in Geophysical Fluid Dynamics (supported by NSF and ONR) at WHOI, where this work began, and the Institute for Mathematics and its Applications (supported by NSF). J-LT was supported by NSF under grant DMS-0806821.

#### REFERENCES

- BOHR, T., DIMON, P. & PUTKARADZE, V. 1993 Shallow-water approach to the circular hydraulic jump. *J. Fluid Mech.* **254**, 635–648.
- BOHR, T., PUTKARADZE, V. & WATANABE, S. 1997 Averaging theory for the structure of hydraulic jumps and separation in laminar free-surface flows. *Phys. Rev. Lett.* **79** (6), 1038–1041.
- BRECHET, Y. & NÉDA, Z. 1999 On the circular hydraulic jump. *American Journal of Physics* **67** (8), 723–731.
- BUSH, J. W. M. & ARISTOFF, J. M. 2003 The influence of surface tension on the circular hydraulic jump. *J. Fluid Mech.* **489**, 229–238.
- CHANG, H.-C., DEMEKHIN, E. A. & TAKHISTOV, P. V. 2001 Circular hydraulic jumps triggered by boundary layer separation. *Journal of Colloid and Interface Science* **233**, 329–338.
- EDWARDS, C. M., HOWISON, S. D., OCKENDON, H. & OCKENDON, J. R. 2008 Nonclassical shallow water flows. *IMA J. Appl. Math.* **73** (1), 137–157.
- GODWIN, R. P. 1993 The hydraulic jump (“shocks” and viscous flow in the kitchen sink). *American Journal of Physics* **61** (8), 829–832.
- GRADECK, M., KOUACHI, A., DANI, A., AMOULT, D. & BORÉAN, J. L. 2006 Experimental and numerical study of the hydraulic jump of an impinging jet on a moving surface. *Exp. Therm. Fluid Sci.* **30**, 193–201.
- KATE, R. P., DAS, P. K. & CHAKRABORTY, S. 2007 Hydraulic jumps due to oblique impingement of circular liquid jets on flat horizontal surfaces. *J. Fluid Mech.* **573**, 247–263.
- KATE, R. P., DAS, P. K. & CHAKRABORTY, S. 2009 Effects of jet obliquity on hydraulic jumps formed by impinging circular liquid jets on a moving horizontal plate. *J. Fluids Eng.* **131** (3), 034502.
- KURIHARA, M. 1946 On hydraulic jumps. *Rep. Research Institute for Fluid Engineering (Kyusyu Imperial University, “Ryutai Kougaku Kenkyusho Kiyou”)* **3**, 11–33, in Japanese.

- LEBON, L., SAGET, B., DURAND, M., LIMAT, L., COUDER, Y. & RECEVEUR, M. 2008 Playing with inclined circular hydraulic jumps. Abstract, 61st Annual Meeting of the APS Division of Fluid Dynamics.
- LISTER, J. R. 1992 Viscous flows down an incline from point and line sources. *J. Fluid Mech.* **242**, 631–653.
- RIENSTRA, S. W. 1996 Thin layer flow along arbitrary curved surfaces. *Z. Angew. Math. Mech.* **76** (S5), 423–424.
- RUBEL, A. 1981 Computation of the oblique impingement of round jets upon a plane wall. *AIAA J.* **19**, 863–871.
- SPARROW, E. M. & LOVELL, B. J. 1980 Heat transfer characteristics of an obliquely impinging circular jet. *ASME, Ser. C: J. Heat Transfer* **102**, 202–209.
- TANI, I. 1949 Water jump in the boundary layer. *J. Phys. Soc. Japan* **4**, 212–215.
- THIFFEAULT, J.-L. & KAMHAWI, K. 2008 Chaotic geodesics. In *Chaos, Complexity, and Transport: Theory and Applications* (ed. C. Chandre, X. Leoncini & G. Zaslavsky). Singapore: World Scientific.
- WATSON, E. J. 1964 The radial spread of a liquid jet over a horizontal plane. *J. Fluid Mech.* **20** (3), 481–499.